Pergamon

Int. J. Heat Mass Transfer. Vol. 39, No. 4, pp. 811–822, 1996

0017-9310/96 $15.00 + 0.00

0017-9310(95)00142-5

An investigation of dependent/independent scattering regimes using a discrete dipole approximation

Ž. IVEZIĆ
Department of Physics and Astronomy, University of Kentucky, Lexington, KY 40506-0055, U.S.A.

and

M. PINAR MENGÜÇ†
Department of Mechanical Engineering, University of Kentucky, Lexington, KY 40506-0046, U.S.A.

(*Received* 22 *July* 1994 *and in final form* 28 *March* 1995)

Abstract—Dependent scattering/independent scattering regimes are investigated in two different particle systems using a discrete dipole approximation for modeling the interaction of electromagnetic waves with the matter. In the first case, absorption and scattering by two small Rayleigh spheres, separated at an arbitrary distance, are discussed and compared against the Lorenz–Mie theory predictions for single spheres. After that, small agglomerates of up to 12 spheres are investigated. Results show that the mutual interaction of two spheres does not affect absorption when the ratio of their distance to the radius, $c = d/a$, is greater than 3. Contrary, an analogous criterion for independent scattering depends on the individual sphere size parameter, x_s, such that it is valid only if $c \geqslant 2/x_s$. It is shown that an agglomerate formed of N individual spheres can be approximated by an effective sphere if $x_e \leqslant 0.2$. For $x_e \approx 2$, agglomerates scatter similar to N independent particles. These limits bracket the true radiative properties of the agglomerates for $0.2 \leqslant x_e \leqslant 2$, where dependent effects cannot be neglected. Additionally, an experimental methodology is suggested to qualitatively identify the process of agglomeration of a number of individual particles even when changes in the number density of particles are unknown.

1. INTRODUCTION

In many high temperature systems, radiation heat transfer is the dominant mode of energy transfer [1, 2]. Radiation is also important in close-packed and insulation systems, where it is usually the only mode of heat transfer [3]. Accurate solutions of the thermal performance of these processes are strongly linked to the solution of the radiative transfer equation, which requires radiative properties of the medium as an input. These are the absorption and scattering coefficients, κ and σ, which are proportional to particles' number density, V_n, and the corresponding cross sections C^{abs} or C^{sca}, and the scattering phase function, $\Phi(\theta)$ [1–3]. Absorption and scattering efficiencies of spherical particles are defined as cross sections normalized by the geometrical cross section, πa^2,

$$Q = \frac{C}{\pi a^2}. \tag{1}$$

Determination of the radiative behavior of the individual spherical particles is a relatively straightforward process [4, 5]. For particle clouds, the total radiative properties can be obtained by using a summation procedure based on the individual particle properties. This approach, called the 'independent scattering' approximation, is acceptable provided that the distances between particles are large compared to the particle dimensions.

If light traverses a perfectly homogeneous medium it is not scattered. Only the inhomogeneities cause scattering. Any material medium has inhomogeneities as it consists of molecules, each of which acts as a scattering center, but it depends on the arrangement of these molecules whether the scattering will be significant. In a perfect crystal at absolute zero temperature, the waves scattered by each molecule interfere in such way as to cause no scattering at all, but just a change in the overall velocity of propagation. For liquids, gases and non-ideal solutions, the thermal movements of the constituent members of the scattering system cause a real scattering. However, thermal movements are not independent and it cannot be expected that the total intensity of scattered light will be a mere summation of the intensities from the individual particles [6]. Some destructive interference will occur and result in a decrease in intensity of scattered light from that expected for independent particles. The assumption of independent scattering implies that

†Author to whom correspondence should be addressed.

NOMENCLATURE

a	radius of each sphere [nm]
c	dimensionless distance between two particles, d/a [—]
d	distance between two particles [nm]
f	function defined by equation (8)
g	function defined by equation (6)
k	imaginary part of refractive index
$\tilde{m}$	complex index of refraction, $n+ik$
n	real part of refractive index
N	number of spheres in an agglomerate
N_{dip}	number of dipoles considered in each sphere
Q	efficiencies, see equation (1) [—]
x	size parameter, $2\pi a/\lambda$ [—].

Greek symbols

α	orientation angle for two spheres, see Fig. 2
β	extinction coefficient ($=\sigma+\kappa$) [m^{-1}]
γ	coefficient defined by equation (21) ($=\sigma/\kappa$) [—]
θ	scattering angle, see Fig. 2
κ	absorption coefficient [m^{-1}]
λ	wavelength [nm]
σ	scattering coefficient [m^{-1}]
Φ	scattering phase function
ψ	orientational angle of scattering plane; see Fig. 2
ω	single scattering albedo, $\sigma/(\sigma+\kappa)$
Δ	fractional accuracy.

Subscripts and superscripts

abs	absorption
agg	agglomerate
e	effective
ind	individual
s	single sphere
sca	scattering
$^-$	normalized quantity.

there is no systematic relation between the phases of waves scattered by different particles. Such assumption can be made if particles are sufficiently far from each other. Early estimates have shown that a mutual distance of three times the radius is sufficient for the assumption of independent scattering [4]. More recently, Tien and his co-workers have modified this approximation to include the wavelength dependence (see ref. [3] for the review). It was also shown that the absorption and scattering cross sections of an agglomerate are different than the corresponding cross-sections of a primary particle multiplied by the total number of particles in the cluster [7–9].

Dependent/independent scattering regimes have been studied by different researchers (see refs. [7–15]), including the most basic system consisting of two approaching spheres. However, these studies were either limited to a very small imaginary part of the refractive index [11, 12], only to conducting spheres [13] or Rayleigh scattering [14], or they were concentrated on a particular effect (e.g. polarization [15]).

In the first part of this work, we investigate the effects of dependent scattering in a system consisting of two spheres at an arbitrary distance with the index of refraction typical for that of soot particles. Our objectives here are: (1) to check the validity of the criterion for independent scattering; (2) to investigate its possible dependence on the size and the arrangement of particles; and (3) to estimate errors introduced by the approximation of independent particles.

The second part deals with closely packed systems of up to 12 spheres where they are either aligned in straight chains or form compact agglomerates. We investigate changes in radiative properties of particles as they agglomerate and suggest methods to identify the process of agglomeration and character of the formed agglomerates. Although there are similar studies in the literature for agglomerates (see refs. [8, 9]), all of them are based on some approximation of the monomers and the EM-wave incident on them. In other words, the dependent effects were not easy to separate from the uncertainties associated with the model itself.

The approach we used here is the discrete dipole approximation, proposed by Purcell and Pennypacker [16], which is currently one of the most general and accurate approaches available for determining the agglomerate properties. The solution scheme we employed is that of Draine [17]. The results were generated using a fixed complex index of refraction value of $\tilde{m} = 1.75+0.75i$, which is similar to that of soot particles generated during the combustion of hydrocarbon fuels. It is important to realize that a more complete study would require a detailed consideration of a larger range of optical properties. Since we focus only on the dependent scattering effects in soot agglomerates, use of a single $\tilde{m}$ value is sufficient and is not going to affect the conclusions drawn here.

2. PROPERTIES OF PARTICLES AND AGGLOMERATES

2.1. *Models for single spheres*

Exact solutions for the absorption and scattering cross-sections and scattering phase function may be determined analytically for simple geometric shapes, such as spheres, by solving the Maxwell equations with boundary conditions corresponding to an infinite plane wave incident on the object. The solution results in an expression involving an infinite series of Ricatti–

Bessel functions [5] and it is known as the Lorenz–Mie theory. For uniform, homogeneous spheres, the solutions may be expressed as a function of the size parameter x and the relative refractive index $\tilde{m} = n+ki$ with respect to the surrounding medium. The size parameter is defined as

$$x = \frac{2\pi a}{\lambda} \tag{2}$$

where a is the radius of the sphere and λ is the wavelength.

For large values of x (for example $x > 200$), the Lorenz–Mie solution converges very slowly. The principles of geometrical optics can be utilized in obtaining the cross-sections and scattering phase function of large spheres (or arbitrary shaped objects). If x is much smaller than unity, the Rayleigh scattering approximation yields the following expressions for the absorption and scattering efficiencies:

$$Q_{abs} = \frac{24nk}{(n^2-k^2+2)^2+4n^2k^2}x \tag{3}$$

$$Q_{sca} = \frac{8}{3}\left|\frac{\tilde{m}^2-1}{\tilde{m}^2+1}\right|^2 x^4. \tag{4}$$

For an agglomerate of arbitrary shape and structure comprised of N spherical particles, absorption and scattering cross-sections can be obtained by formulating the interaction of EM-wave with the matter. The discrete dipole (or coupled dipole) approximation is such a semi-microscopic analysis applicable for the solution of these type of problems [16, 17].

2.2. *Discrete dipole approximation for agglomerates*

Discrete dipole approximation (DDA) has proven to be a very flexible and general technique for calculating the optical properties of particles of arbitrary shapes [17]. The DDA replaces the solid particle with an array of N point dipoles. The spacing between the dipoles is small compared to wavelength. Each dipole has an oscillating polarization in response to both the incident plane wave and the electric field, due to all of the other dipoles in the array. A self-consistent solution for the dipole polarizations can be obtained as the solution to a set of coupled, complex, linear equations.

The DDA is especially suited to scattering characterized by small values of the size parameter x, and shares many of the conceptual features of the Rayleigh approximation [17–19]. However, it is not without limitations. The solution of equations requires the inversion of a matrix with considerably large dimensions. Some of the other algorithms used for the same purpose fail for strongly absorptive refractive indices [17]. The effect of the surface granularity affects the accuracy of the calculations and sets the lower limit on the number of used discrete dipoles. Draine [17], set up a criterion for minimum number of dipoles as

$$N \geqslant \frac{4\pi}{3}x^3|\tilde{m}|\left(\frac{0.1}{\Delta}\right)^3 \tag{5}$$

where Δ is desired fractional accuracy (or relative error normalized to unity; i.e. 1% = 0.01). For example, with $|\tilde{m}| = 1.75+0.75i$ used in this work and $x = 2$, desired accuracy of 0.1 (10%) is achieved with $N > 64$. It should be noted that this criterion is necessary but not sufficient if $|\tilde{m}|$ is large enough, because of magnetic dipole absorption. However, for $|\tilde{m}|$ used in this work, this effect is negligibly small. For a detailed discussion of the application of equation (5), the reader is referred to Draine's work [17].

Given its flexibility, the DDA can be used effectively to investigate radiative properties of arbitrarily shaped particles and agglomerates. The recent reviews of this approach were given in refs. [17–21]; therefore, there is no need to discuss the details here.

3. DEPENDENT/INDEPENDENT SCATTERING LIMITS

Although DDA can simulate arbitrary agglomerates with good accuracy, it is computationally expensive and cannot be readily expanded to large systems. Because of this, it is preferable to follow a simpler methodology to predict the radiative properties of agglomerates and irregularly shaped particles. For example, if the properties of agglomerates can be correlated in terms of those of smooth, homogeneous spheres, then the Lorenz–Mie theory could be employed to calculate the necessary properties. Indeed this has been the general approach taken for most practical systems (see refs. [1, 8, 9] for the reviews). It is important to note here that, with the availability of better computer hardware and algorithms, it will be easier to perform rigorous calculations based on agglomerates. However, there is a need to simplify these calculations as much as possible for use in complex systems, such as in furnace design. Then, one of the most important questions is, 'Under what conditions can an agglomerate be simulated as a homogeneous sphere?' Another question to be answered is 'When can a N-particle agglomerate be represented by N independent particles?' The answers to these questions will reveal the border between dependent and independent scattering regimes.

In general, absorption-scattering cross-sections of a N-particle agglomerate can be expressed in terms of equivalent sphere properties as

$$C^N = \pi a_e^2 Q_1(x_e) g(x_e, N) \tag{6}$$

where a_e, x_e and $Q_1(x_e)$ are radius, size parameter and absorption or scattering efficiency, respectively, of a sphere with the same volume as the N particle cluster. That is,

$$a_e = a_s N^{1/3} \tag{7}$$

where a_s is the radius of the primary spheres. Effects

of the shape, structure and mutual interaction between the monomers are contained in the function $g(x_e, N)$. Parameters a_e and x_e do not change during the process of agglomeration of N particles, which is fully described by the changes of $g(x_e, N)$. If C^N is the true cross-section of an agglomerate, the g-function represents the fractional error introduced by the assumption of a single effective particle, which is described by an equivalent sphere radius of a_e. A similar approach was also suggested by Ku and Shim [8] for agglomerates, although they did not elaborate on the functional dependencies.

If g is equal to 1 for both absorption and scattering cross-sections, then the effective sphere is a good model for the agglomerate. Such radiative behavior can also be considered as the asymptotic limit for the dependent scattering regime. This limit is achieved if the wavelength of radiation is large with respect to the size of the monomers of the agglomerate or the granularity of the surface (as opposed to a smooth, homogeneous sphere) and, hence, structural details cannot be resolved. As the size of individual spheres (monomers) increases, we expect that a single effective sphere model begins to fail and the g-functions deviate from unity. We can determine the g functions by dividing the actual cross-section of the agglomerate, calculated, for example, using the DDA, with that of the effective sphere obtained from the Lorenz–Mie theory.

An equivalent expression for the cross section of the agglomerated particle can be given using the single sphere properties. Analogous to equation (6), we can write:

$$C^N = N\pi a_s^2 Q_1(x_s) f(x_s, N). \tag{8}$$

Here a_s and x_s are the radius and size parameter of single spheres which make the agglomerate. If the particles are scattering completely independently, then the f-functions have the asymptotic limits of unity. Such limit is expected only if the distance between the particles is larger than the wavelength of the incident radiation. As the particles approach and begin to interact with each other, as during the agglomeration process, f-functions deviate from this asymptotic limit of 1. Similar to g functions, f functions can be obtained from comparison of DDA and the Lorenz–Mie theory results. Note that $g(x_e, N)$ and $f(x_s, N)$ correspond to either g^{abs} and f^{abs} or to g^{sca} and f^{sca}, and are related to each other as

$$g(x_e, N) = \frac{Q_1(x_s = x_e N^{-1/3})}{Q_1(x_e)} \times f(x_s = x_e N^{-1/3}, N) \times N^{1/3}. \tag{9}$$

If both x_s and $x_e \ll 1$, deviations of $g(x_e, N)$ when the effective sphere model is not applicable and $f(x_s, N)$ when interaction between the individual spheres is not negligible, can be predicted theoretically. At this limit, using the Rayleigh approximation [equations (3) and (4)], we can write

$$\left[\frac{Q_1(x_s)}{Q_1(x_e)}\right]^{abs} = \frac{a_s}{a_e} = N^{-1/3} \tag{10}$$

$$\left[\frac{Q_1(x_s)}{Q_1(x_e)}\right]^{sca} = \left(\frac{a_s}{a_e}\right)^4 = N^{-4/3}. \tag{11}$$

If all N particles of an agglomerate interact with the incoming radiation *independently* of each other, then

$$C^N = N\pi a_s^2 Q_1(x_s) \tag{12}$$

and from equation (8)

$$f^{abs}(x_s, N) = 1 \tag{13}$$

$$f^{sca}(x_s, N) = 1. \tag{14}$$

Using equations (9)–(11), we obtain for the independent scattering regime of Rayleigh particles (both individual and effective spheres)

$$g^{abs}(x_e, N) = 1 \tag{15}$$

$$g^{sca}(x_e, N) = \frac{1}{N}. \tag{16}$$

Contrarily, if all N particles of an agglomerate are assumed to *merge together* and act as a single homogeneous spherical particle with radius a_e, we can write from equation (6)

$$g^{abs}(x_e, N) = 1 \tag{17}$$

$$g^{sca}(x_e, N) = 1. \tag{18}$$

Following equation (9)–(11) we find for Rayleigh particles

$$f^{abs}(x_s, N) = 1 \tag{19}$$

$$f^{sca}(x_s, N) = N. \tag{20}$$

Note that these theoretical results are for small x_e and x_s values. It is obvious that scattering properties are more suitable than the absorption properties to investigate dependent effects and agglomeration.

The requirement for small Rayleigh size particles (i.e. $x \leqslant 1.0$) is easily met for individual soot particles, whose sizes are in the order of 20–50 nm, if the wavelength of interest is at the visible or infrared spectrum. For agglomerates, however, Rayleigh approximation needs to be replaced with the Lorenz–Mie calculations, which requires the modification of equations (10) and (11). For this case, equations (13), (14) and (17), (18) are still valid by definition. The new forms of f and g function limits given by equations (15), (16) and (19), (20) depend on the size parameter. These relations are calculated from the Lorenz–Mie theory and depicted in Fig. 1. The left panels of this figure show the f-functions for effective sphere approximation (a dependent scattering asymptote, as discussed before). These functional variations should replace the limits given by equations (19) and (20). The right panels of Fig. 1 depict g^{abs} and g^{sca}, if the particles in N-particle agglomerate scatter independently and replace equations (15) and (16). These

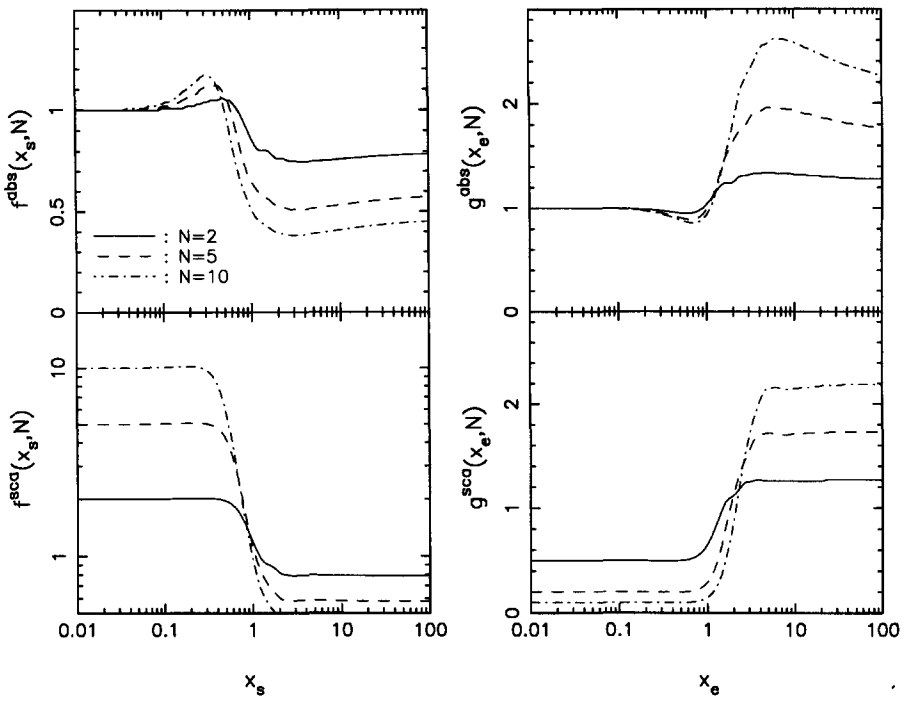

Fig. 1. Behavior of f and g functions (see text) obtained from the Lorenz–Mie theory for $\tilde{m} = 1.75+0.75i$. Number of single spheres that form an equivalent sphere, N, is 2 (solid line), 5 (dashed line) and 10 (dot–dashed line).

results indicate that absorption and scattering cross-sections can be represented with the Rayleigh approximation (within 10%), i.e. with equations (15), (16), (19) and (20), as long as $x_s \leqslant 0.3$ or $x_e \leqslant 1$.

4. RESULTS AND DISCUSSIONS

In order to obtain the agglomerate properties, the discrete dipole approximation algorithm (called DDSCAT) developed by Draine [17] was used. All runs were performed on an IBM 3090-600J computer. Initial computer simulations were made for a single sphere in order to obtain the minimal number of dipoles, N_{dip}, needed to get a good agreement with the results from the Lorenz–Mie theory. For $N_{dip} = 123$ and $x < 2$, results from DDA were within 10% from the exact values obtained by the Lorenz–Mie theory, in agreement with equation (5). Analogous computations with $N_{dip} = 515$ did not show a significant decrease of error for $x \leqslant 2$. These observations are in agreement with those reported by Draine [17] and, therefore, there is no need to further discuss them here.

4.1. *Two spheres*

In this section, we will investigate the radiative properties of two spheres separated by a normalized distance of $c = d/a$, where d is the distance between the spheres (surface to surface) and a is their radius. It is assumed that each sphere consists of 123 dipoles, and c is varied from 0 to 100. Complex index of refraction was assumed constant and taken as $\tilde{m} = 1.75+0.75i$. This is a value typical for soot particles produced during combustion of hydrocarbon fuels [1, 8]. The angle between the line connecting the spheres and the direction of incident light, α, was taken as either 0° (back to back spheres, with respect to the Poynting vector) and 90° (side by side spheres; see Fig. 2). Two initial polarizations were chosen for $\alpha = 90°$; parallel to the line connecting the spheres (polarization 1) and perpendicular to it (polarization 2). In calculating the f and g functions, the Lorenz–Mie theory was used to determine both the individual and agglomerate sphere properties for all size parameters. Therefore, they are not based on simplified Rayleigh sphere properties.

Note that two isolated spheres do not represent a real system. Our results can be used as a criterion for minimal distance between the closest neighbors for the assumption of independent interaction with the incident radiation. If the closest neighbors do not interact mutually, then it is safe to assume that more distant particles do not interact either.

Figure 3 depicts $g^{abs}(x_e, 2)$ and $g^{sca}(x_e, 2)$ for $c = 0$, 3 and 10 (dotted, dashed and solid lines, respectively) and two orientations of the incident radiation. In agreement with previous estimates, g^{abs} is essentially 1 (within 5%) for $c \geqslant 3$ and all size parameters, while for $c = 0$ it differs from unity as much as 40% for $x_e = 0.2$, polarization 1, $\alpha = 90°$. Therefore, we can safely claim that the absorption of radiation is not altered by the mutual interaction of the spheres considered here when $c > 3$.

It is important to note that our calculations for c

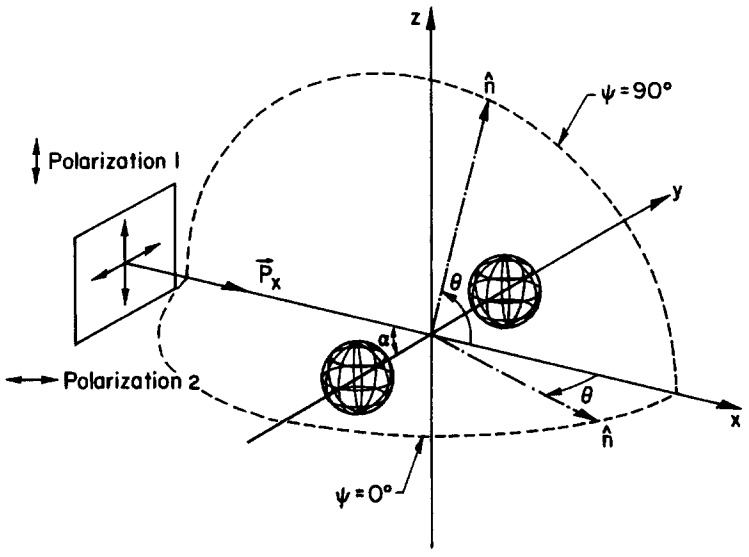

Fig. 2. Coordinate system, orientation of the incident EM wave, and scattering planes used in computations of the scattering and absorption properties for a system consisting of two spheres at an arbitrary distance.

values of 0, 3 and 10 were not chosen arbitrarily. The calculations were first performed for several c values between 0 and 100 for two-sphere systems, with $x_s = 0.2$ and 1.0, and 515 dipoles in each sphere. Absorption and scattering cross sections for two orthogonal polarization states of the incident beam were determined and compared. When the two-sphere model cannot be represented as two independent spheres, the results based on two polarizations are expected to differ. Contrarily, if they are independent scatterers, the results should not be affected by the polarization of the incident radiation. Indeed, our cal-

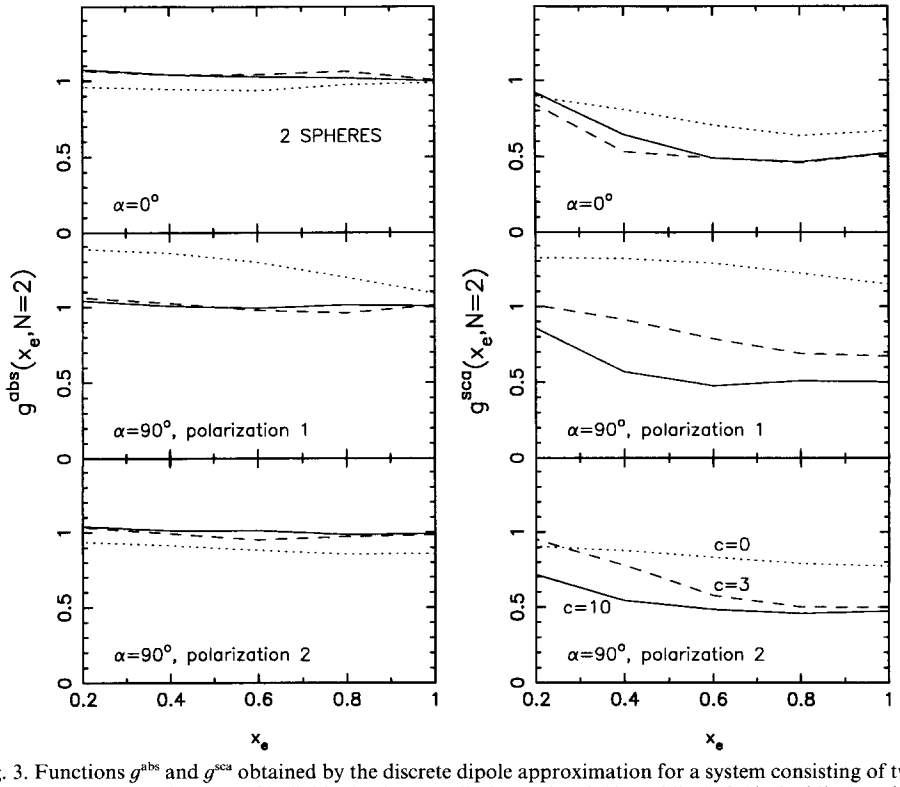

Fig. 3. Functions g^{abs} and g^{sca} obtained by the discrete dipole approximation for a system consisting of two spheres at distance c (in units of individual spheres radius) equal to 0 (dotted line), 3 (dashed line) and 10 (solid line). Angle α is the angle between the line connecting the spheres and direction of the Poynting vector. When $\alpha = 90°$, *polarization* 1 denotes the electric vector parallel to the line connecting the spheres, while *polarization* 2 is the perpendicular polarization.

culations revealed that for $c \leqslant 3$ the efficiencies were different and for higher values they approached each other asymptotically. There was virtually no difference in efficiencies for the parallel and perpendicular polarizations when c was increased from 10 to 100. Based on these comparisons only three c values, 0 for touching spheres, 10 for independent regime and 3 for change in functional behavior of efficiencies, were considered in later work.

The expected value for g^{sca} is 0.5 ($= 1/N$) in the Rayleigh limit when scattering is independent, while for a single unified particle $g^{sca} = 1$. The right panel of the Fig. 3 shows that g^{sca} does approach the value of 0.5 when $x_e \approx 1$ and $c \geqslant 3$. For smaller x_e and c values, g^{sca} increases. For example, if $x_e \approx 0.2$ and $c < 3$, g^{sca} is close to 1, which is the value expected for two spheres acting as a single particle. If the particles are touching each other, i.e. $c = 0$, g^{sca} is significantly larger than the asymptotic value of 0.5 for all x_e, meaning independent scattering cannot represent the true physics of the problem at all (however, it is possible to use the effective sphere model, or dependent scattering regime, if particles are small, i.e. $x_e \leqslant 0.2$).

The criterion for independent scattering depends on the size parameter, x_e, such that $c \geqslant 3$ criterion is valid only if $x_e \geqslant 0.8$ (with maximal allowed difference in g^{sca} of 10%, see right panel of Fig. 3). It is clear that for a sufficiently small size parameter, the scattering is asymptotically *dependent*, i.e. the spheres interact with the radiation as if they were a single homogeneous particle. This is not surprising since, for $c \leqslant c_{min} \approx 2.4/x_e \approx 2/x_s$, the wavelength of the incident radiation exceeds the overall size of the system and the incident EM wave cannot distinguish the structure of the system.

Figure 4 shows phase function, $\Phi(\theta)$, averaged over both polarizations, for $x_e = 0.2$ and two orientations of the incident EM wave. For $\alpha = 90°$, $\Phi(\theta)$ is presented in the plane which contains both spheres ($\psi = 0°$, solid line) or in the perpendicular plane ($\psi = 90°$, dotted line). For $\alpha = 0°$, the system is axially symmetric and all scattering planes are equivalent. As a comparison, we plot $\Phi(\theta)$ for a single sphere of the same size parameter determined from the Lorenz–Mie theory (dashed line).

Dependent scattering is related to both the distance between the spheres, c, and the orientation of the axis connecting the spheres with respect to incident radiation.

For $c = 0$ and $\alpha = 0°$, the spheres are oriented back-to-back and they show slightly more (53%) forward scattering ($\theta < 90°$) at the expense of the backward one ($\theta > 90°$). This deviation increases with c and, for $c = 10$, 90% of the incident radiation is scattered forward. When $c = 100$, the peaks of wiggles caused by interference effects become profound and oscillate around the phase function for a single sphere. Although forward and backward scattered radiation are equal, more radiation is scattered sideway ($45° < \theta < 135°$) than in the single sphere case. The

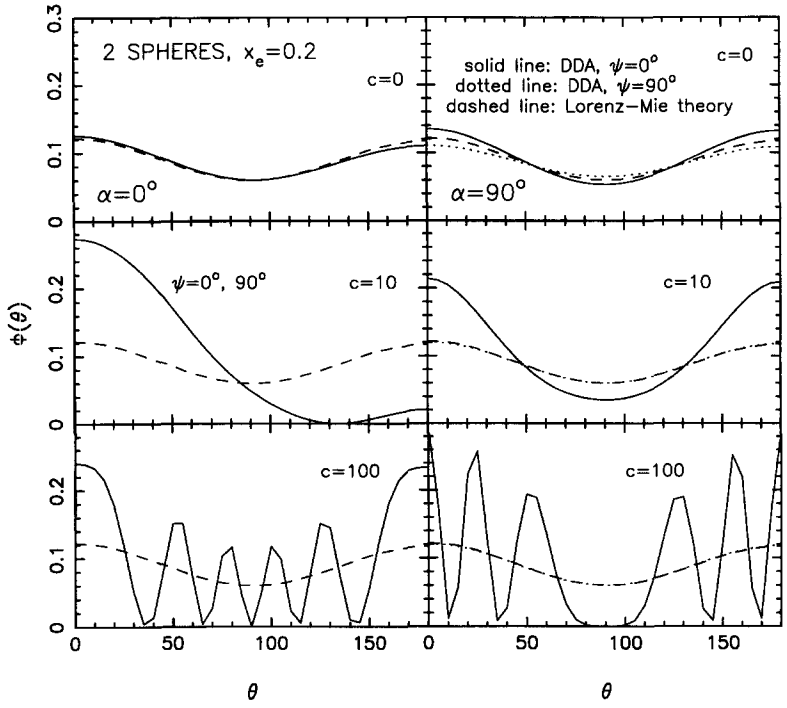

Fig. 4. Results for the scattering phase function averaged over two polarizations for the two spheres system and $x_e = 0.2$. Symbols are the same as in Fig. 3. Angle ψ is the angle between the scattering plane and xy plane (see Fig. 2). Dashed line is the phase function for a sphere with the same effective size, obtained from the Lorenz–Mie theory. Solid and dotted lines are phase functions for $\psi = 0$ and 90°, respectively (note that for $\alpha = 0°$ both lines are identical because of symmetry).

observed trend shows that, for even greater c, $\Phi(\theta)$ smoothed over θ would fall onto $\Phi(\theta)$ for a single sphere. Such behavior is indeed expected, since this is an analogous situation to the smoothing of a diffraction pattern when the angular resolution is not sufficient and/or the slit spacing is too large.

For $\alpha = 90°$ (right panel of Fig. 4), $\Phi(\theta)$ for two spheres is symmetric with respect to $\theta = 90°$ but shows differences in side scattering compared to a single sphere, depending on ψ-angle. It can be assumed, since deviations from the $\Phi(\theta)$ for a single sphere are not large in either of the three cases, that, even for $c = 0$, the angular distribution of the scattered radiation resembles that for a single sphere. As c increases, $\Phi(\theta)$ for $\psi = 90°$ approaches $\Phi(\theta)$ for a single sphere. There are no interference effects for this orientation since the scattering plane for $\psi = 90°$ is the plane of symmetry and all points in the plane are at the same distance from both spheres. Interference analogous to the case $\alpha = 0°$ can be seen for $c = 100$ and $\psi = 0°$ at $\alpha = 90°$.

Since in real systems there are many spheres with random relative orientations, deviations in phase function would be hard to observe for large c values. It can be expected, however, that as the spheres approach each other we would see changes in forward, side and backward scattering.

4.2. *Clusters of* N *spheres*

Effects of clustering were investigated for two types of systems consisting of N spheres ($N \leqslant 12$): aligned spheres and closely packed agglomerates (e.g. tetrahedron for $N = 4$, body centered tetrahedron for $N = 5$, body centered cube for $N = 9$, a cube with two spheres attached at two opposite sides for $N = 10$, etc.). Since efficiencies and the scattering pattern depend on polarization of the incident light and orientation of the system, all results are averaged over these parameters.

If agglomerates can be approximated as single effective spheres, $g^{sca}(x_e, N)$ and $g^{abs}(x_e, N)$ are close to unity, while $f^{sca}(x_s, N)$ and $f^{abs}(x_s, N)$ should show the behavior depicted in the left panels of Fig. 1. Contrarily, if all N particles interact independently with the incident radiation, $f^{sca}(x_s, N)$ and $f^{abs}(x_s, N)$ are unity and $g^{sca}(x_e, N)$ and $g^{abs}(x_e, N)$ follow the behavior depicted in the right panels of Fig. 1.

Results for $g(x_e, N)$ and $f(x_s, N)$ are shown in Fig. 5. Solid lines represent compact systems while dashed lines correspond to linear systems with number of constituent spheres, N, as listed in the inset. The agglomerate calculations could not be carried out beyond $x_s \approx 1$ due to the computational difficulties.

The behavior of f^{abs} and f^{sca} for agglomerates, as depicted in Fig. 5, is almost identical to that of f^{abs} and f^{sca} shown in Fig. 1 for spherical particles. Two upper panels for f^{abs} and g^{abs} show that absorption of the incident radiation is not affected much by the mutual interaction of the constituent particles, nor by the deviations from the spherical shape (within 20% variation) for $x_e \leqslant 1.0$ [or corresponding x_s as a function of N, see equations (2) and (7)]. However, for $x_e > 1.0$, $g^{abs}(x_e, N)$ increases with x_e, an effect pro-

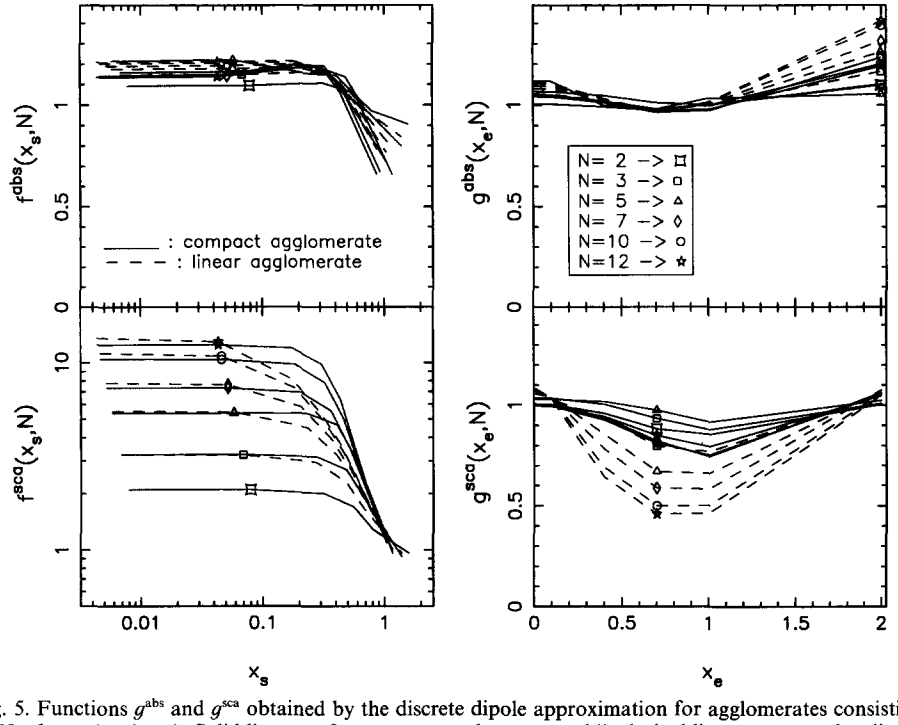

Fig. 5. Functions g^{abs} and g^{sca} obtained by the discrete dipole approximation for agglomerates consisting of N spheres (see inset). Solid lines are for compact agglomerates while dashed lines correspond to linear shapes (aligned spheres).

portional to N and more profound for linear agglomerates. For $x_e \geqslant 1$, such behavior is indeed expected, as can be seen from the g^{abs} profiles given in Fig. 1. It is worth noting that the asymptotic limit $g^{abs} = 1$ is not valid here, as x_s is large for reliable use of Rayleigh regime values. Instead, Fig. 1 should be considered.

There are larger differences between the scattering behavior of independent scatterers and modeled agglomerates. The lower panels of the Fig. 5 show that, if $x_e \leqslant 0.2$, scattering is asymptotically dependent ($g^{sca} \approx 1, f^{sca} \approx N$) and the single unified particle model works well.

Although minor differences exist for large N between the two types of the agglomerates, their scattering behavior is qualitatively the same. In agreement with previous studies, results presented in Fig. 5 show that all agglomerates can be approximated within 10% by the model of an effective sphere when $x_e \leqslant 0.2$. As the size parameter increases, the error introduced by the approximation of effective spheres also increases, because the wavelength of the incident radiation begins to "see" the structure, i.e. at this range g^{sca} deviates from unity. If the spheres were beginning to scatter independently, then the corresponding g^{sca} function should approach the profiles depicted in the lower right panel of Fig. 1 (for independent scattering in the Rayleigh limit $g^{sca} = 1/N$). With even further increase of x_e beyond 1, $g^{sca}(x_e, N)$ increases too, and becomes almost identical to the value at $x_e = 2$ for a system of N independent spheres (lower right panel of Fig. 1). At x_e values beyond 2, g^{sca} for independent scatterers approach constant, N dependent, values. The agglomerates are likely to approach this limit too, but we cannot determine it from the DDA calculations.

The dependent effects never disappear from agglomerates as depicted in the lower, right panel of the Fig. 5. This was already shown in the analysis of the two spheres system where, for $c = 0$ (as in agglomerates), the scattering is never independent. Anyway, for $x_e \approx 2$ the difference between g^{sca} calculated for agglomerates and g^{sca} for N independent spheres is 10–20%. Thus, for this x_e value, model of N independent spheres can be used to predict radiative properties of agglomerates. In a region where neither of the two models work, $0.2 \leqslant x_e \leqslant 2$, we can assume that the true values of radiative properties are somewhere between the limits given by these models. In this region, the models disagree by about a factor of 2 for scattering. The true difference depends on x_e, shape of the agglomerate, number of the constituent spheres and, presumably, the index of refraction.

4.3. *Identification of the agglomeration process*

The results from Fig. 5 can also be used to trace the process of agglomeration of N individual particles into an agglomerated particle. As N particles agglomerate, the particle number density, V_n, decreases. This change is reflected in the macroscopic radiative properties, κ and σ. In order to investigate the effects of agglomeration only on the radiative properties, the effects of changes in V_n must be excluded. A convenient measurable quantity to trace the agglomeration process and which does not depend on V_n is the ratio σ/κ:

$$\gamma = \frac{\sigma}{\kappa} = \frac{\omega}{1-\omega} = \frac{C^{sca}}{C^{abs}} = \frac{Q_1^{sca}(x_e)\, g^{sca}(x_e, N)}{Q_1^{abs}(x_e)\, g^{abs}(x_e, N)} = \frac{Q_1^{sca}(x_s)}{Q_1^{abs}(x_s)} \frac{f^{sca}(x_s, N)}{f^{abs}(x_s, N)} \quad (21)$$

where ω is the single scattering albedo. Note that the two relations given in equation (21) are equivalent, since the f and g functions are not independent [see equation (9)]. If we assume that, before the agglomeration takes place, all N particles are independent, than the ratio γ will be different after the agglomeration. For $x_e \leqslant 0.2$, γ will increase proportionally to N, and $\bar{\gamma} = \gamma^{agg}/\gamma^{ind} \approx N$ where γ^{agg} and γ^{ind} stand for γ after and before the agglomeration takes place, respectively. This behavior for small particles was also observed by Ku and Shim [7].

If the individual particles cannot be considered independent scatterers before the agglomeration (if the distance between the closest neighbors is not greater than $2x_s$, see Section 4.1), we can still expect some increase in $\bar{\gamma}$ as an indication of the ongoing agglomeration process. The expected ratio $\gamma^{agg}/\gamma^{ind}$ when condition $x_e \leqslant 0.2$ is not met is shown in Fig. 6 as a function of x_s and x_e—note that

$$\bar{\gamma} = \left[\frac{f^{sca}(x_s, N)}{f^{abs}(x_s, N)}\right]^{agg} \quad \text{since} \quad \left[\frac{f^{sca}(x_s, N)}{f^{abs}(x_s, N)}\right]^{ind} = 1.$$

As evident from the right panel, $\bar{\gamma} \approx N$ is correct within 10–20% for $x_e < 0.5$. Even when $x_e \approx 1.5$ there is a clear increase in $\bar{\gamma}$. Thus, increase of $\bar{\gamma}$ can be considered as the sign of the agglomeration process. Furthermore, if $\tilde{m}(\lambda)$ is available and once the agglomeration is observed, multi-wavelength measurements can provide an estimate of x_s and N by identifying the steep decrease in $\gamma^{agg}/\gamma^{ind}$, shown in the left panel of Fig. 6. Hence, the agglomeration process can be traced and, as well, size and number of agglomerated particles can be estimated. However, the structure of agglomerates cannot be determined by measurements of $\bar{\gamma}$, since $\bar{\gamma}$ does not appear to be dependent on the agglomerates' shape.

An insight into the structure of the agglomerated particles can be obtained from the phase function. Figure 7 shows $\Phi(\theta)$ for agglomerates consisting of 3, 7 and 12 spheres and various x_e as marked. We display the phase function normalized by its value at $\theta = 0°$ because it is easier to distinguish the results for different x_e values.

Compact agglomerates scatter more radiation forwards than linear agglomerates do, with the differences proportional to the number of agglomerated particles (77% for compact and 65% for linear agglomerates when $N = 12$). The shape of the phase

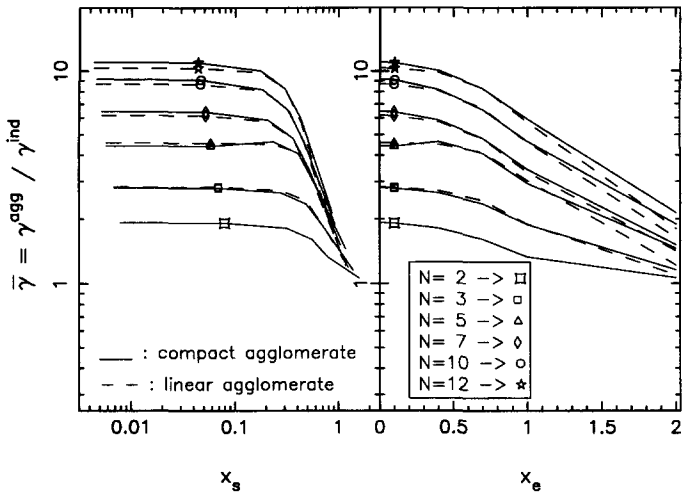

Fig. 6. Ratio $\bar{\gamma} = \gamma^{agg}/\gamma^{ind}$ as a function of x_s and x_e. γ^{agg} and γ^{ind} stand for $\gamma = \sigma/\kappa$ after and before the agglomeration takes place, respectively.

function at angles beyond 150° can also be used to determine x_e, if all agglomerates are similar. Thus, by simultaneous measurements of the ratio σ/κ and the phase function $\Phi(\theta)$, both the number of agglomerated particles and the structure of the formed agglomerates can be determined, at least qualitatively.

We find that an additional difference in radiative behavior of the two types of agglomerates can be seen in measurements of the depolarization. While compact agglomerates do not depolarize incident radiation (<1%), linear systems depolarize about 10% of the back-scattered ($\theta > 90°$) radiation, independently of the number of agglomerated particles.

We have also investigated the behavior of agglomerates regarding the polarization. We find that polarization of the scattered radiation is very small and basically the same for both types of the agglomerates. Thus, polarization measurements are not expected to be a good tracer of the agglomeration process and agglomerates morphology.

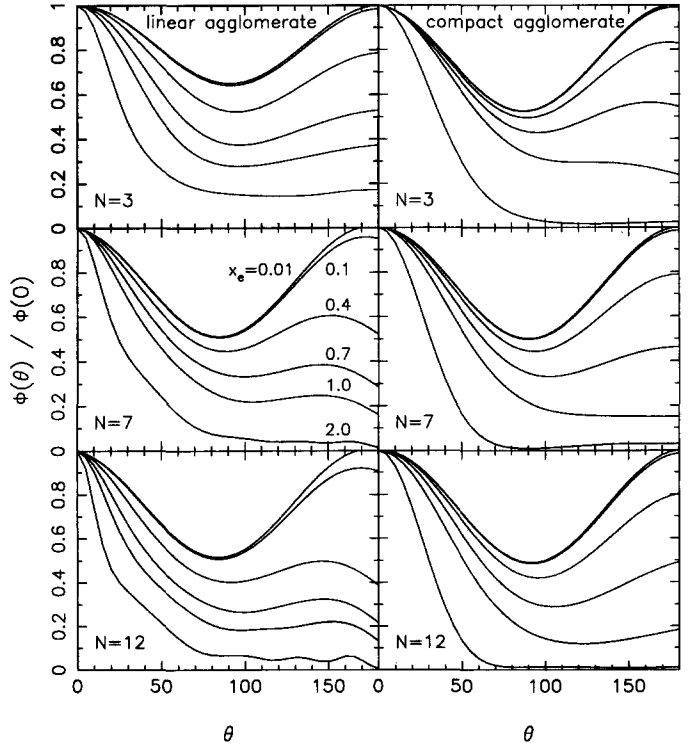

Fig. 7. Phase functions for agglomerates consisting of N spheres.

Structures of the agglomerates used in this work represent limiting cases. It is likely that real agglomerates will be different and somewhere between the structures considered. Also, the number of spheres considered in each agglomerate was limited because of the computational difficulties. However, the results indicate that $N = 12$ is not far from asymptotic limit for the complex index of refraction used. The presence of more particles would not alter our discussion of dependent effects.

5. CONCLUSIONS

Although in most radiation heat transfer applications independent scattering is a valid assumption, for some scattering media (e.g. agglomerates, microsphere insulations) dependent scattering must be taken into account. Also, for accurate interpretation of light extinction/scattering experiments to understand, for example, soot formation and coagulation processes, the dependent scattering regime needs to be identified clearly. Analysis based on a discrete dipole approximation shows that, for a system consisting of two spheres, absorption of the incident radiation is essentially independent when the distance between the spheres, d, is larger than three times the radius a of a single sphere. An analogous criterion for independent scattering depends on the single particle size parameter, x_s, and normalized distance between the particles, c. It is approximately given as $c \geqslant 2/x_s \approx 2.4/x_e$. Hence, there is always a sufficiently small x_s which allows the use of an effective sphere approximation (which is a form of dependent scattering). The limit for the independent/dependent regime can also be expressed as $d \geqslant \lambda/\pi$.

Results averaged over orientations of the particles and polarizations of the incident radiation show that arbitrarily shaped agglomerates consisting of N individual spheres can be approximated as an effective sphere if $x_e \leqslant 0.2$. For $x_e \approx 2$, agglomerates give the same scattering cross-sections as N independent particles. In the intermediate region where agglomerates cannot be approximated by either of these two models, model predictions differ by about a factor of two for $N \leqslant 12$ and index of refraction used in this work. It can be assumed that results obtained in these two limiting cases bracket the true radiative properties of the agglomerates for $0.2 \leqslant x_e \leqslant 2$. In this range, the use of agglomerate models is recommended.

Analysis of the calculated optical properties of agglomerates show that the agglomeration process of N individual spheres into a linear or compact agglomerate can be identified. The agglomeration process can be followed, even if the changes in the overall number density are not known. Simultaneous measurements of the ratio σ/κ and the phase function can be used to determine the number of the agglomerated particles, their size and the structure of the formed agglomerate. In a hostile flame environment, however, these changes may not be easy to capture. A more detailed study of this possibility is already underway.

Acknowledgements—This research project has been supported by the DOE-PETC Advanced University Coal Research Program Grant no: DE-FG22-PC92533. We also thank Drs B. T. Draine and P. J. Flatau for supplying the original version of the DDSCAT algorithm used here for the DDA calculations. Constructive criticism of anonymous reviewers helped us to improve the paper; we acknowledge their contribution. The computations were performed using the IBM 3090-600J supercomputer at the University of Kentucky.

REFERENCES

1. R. Viskanta and M. P. Mengüç, Radiation heat transfer in combustion systems, *Prog. Energy Combust. Sci.* **13,** 97–160 (1987).
2. R. Siegel and J. R. Howell, *Thermal Radiation Heat Transfer*, 3rd Edn. Hemisphere Washington DC (1993).
3. C. L. Tien, Thermal radiation in packed and fluidized beds, *J. Heat Transfer* **110,** 1230–1242 (1988).
4. H. C. van de Hulst, *Light Scattering by Small Particles* (1st Edn). Dover, New York (1981).
5. C. F. Bohren and E. R. Huffman, *Absorption and Scattering of Light by Small Particles* (2nd Edn). Wiley, New York (1983).
6. G. Oster, The scattering of light and its applications to chemistry, *Chem. Rev.* **43,** 319–323 (1948).
7. B. L. Drolen and C. L. Tien, Absorption and scattering of agglomerated soot particulate, *J. Quant. Spectrosc. Radiat. Transfer* **37,** 433–448 (1987).
8. J. C. Ku, and K.-H. Shim, The effects of refractive indices, size distribution, and agglomeration on the diagnostics and radiative properties of flame soot particles. In: *Heat and Mass Transfer in Fires and Combustion Systems* (Edited by W. L. Grosshandler and H. G. Semerjian), ASME HTD-148, pp. 105–115. ASME, New York (1990).
9. J. C. Ku, and K.-H. Shim, A comparison of solutions for light scattering and absorption by agglomerated or arbitrarily-shaped particles, *J. Quant. Spectrosc. Radiat. Transfer* **47,** 201–220 (1992).
10. S. Kumar and C. L. Tien, Dependent scattering and absorption of radiation by small particles, *Proceedings of the 24th National Heat Transfer Conference*, HTD-Vol. 72, pp. 1–7 (1987).
11. D. W. Mackowski, Analysis of radiative scattering for multiple sphere configurations, *Proc. R. Soc. Lond.* **A 433,** 599–614 (1991).
12. F. Borghese, P. Denti, R. Saija, G. Toscano and O. I. Sindoni, Multiple electromagnetic scattering for a cluster of spheres. I. Theory, *Aerosol Sci. Technol.* **3,** 227–235 (1984).
13. J. H. Bruning and Y. T. Lo, Multiple scattering of EM waves by spheres Part I—Multipole expansion and ray-optical solutions, *IEEE Trans. Ant. Prop.* **3,** 378–400 (1971).
14. G. O. Olaofe, Scattering cross-section for two spheres, *Q. J. Mech. Appl. Math.* **27,** 403–422 (1974).
15. J. C. Ravey, Light scattering by aggregates of small dielectric or absorbing spheres, *J. Coll. Interface Sci.* **46,** 139–146 (1974).
16. E. M. Purcell and C. R. Pennypacker, Scattering and absorption by non-spherical dielectric grains, *Astrophys. J.* **186,** 705–714 (1973).
17. B. T. Draine, The discrete dipole approximation and its application to interstellar graphite grains, *Astrophys. J.* **333,** 848–872 (1988).
18. P. J. Flatau, G. L. Stephens and B. T. Draine, Light scattering by rectangular solids in the discrete-dipole

approximation: a new algorithm exploiting the Block-Toeplitz structure, *J. Opt. Soc. Am.* **A7,** 593–600 (1990).
19. P. J. Flatau, Scattering by irregular particles in anomalous diffraction and discrete dipole approximation, Ph.D. Thesis, Colorado State University, Fort Collins, CO (1992).
20. A. Lakhtakia, Macroscopic theory of the coupled dipole approximation method, *Opt. Commun.* **79,** 1–5 (1990).
21. M. P. Mengüç, A. Mahadevia, K. Saito and S. Manickavasagam, Application of discrete dipole approximation to sooting diffusion flames, *ASME National Heat Transfer Conference*, San Diego, CA (1992).